Available online at www.sciencedirect.com
ScienceDirect
Geochimica et Cosmochimica Acta 72 (2008) 2754–2766
Geochimica et Cosmochimica Acta
www.elsevier.com/locate/gca

Dissolution of arsenopyrite (FeAsS) and galena (PbS) in the presence of desferrioxamine-B at pH 5

Hilda Cornejo-Garrido [a,b], Pilar Fernández-Lomelín [b], José Guzmán [c], Javiera Cervini-Silva [b,*]

[a] *Facultad de Química, Universidad Nacional Autónoma de México, Cd. Universitaria, México D. F. CP 04510, México*
[b] *Instituto de Geografía, Universidad Nacional Autónoma de México, Cd. Universitaria, México D. F. CP 04510, México*
[c] *Instituto de Investigación en Materiales, Universidad Nacional Autónoma de México, Cd. Universitaria, México D. F. CP 04510, México*

Received 16 October 2007; accepted in revised form 19 February 2008; available online 29 February 2008

Abstract

Microorganisms and higher plants produce biogenic ligands, such as siderophores, to mobilize Fe that otherwise would be unavailable. In this paper, we study the stability of arsenopyrite (FeAsS), one of the most important natural sources of arsenic on Earth, in the presence of desferrioxamine (DFO-B), a common siderophore ligand, at pH 5. Arsenopyrite specimens from mines in Panasqueira, Portugal (100–149 μm) that contained incrustations of Pb, corresponding to elemental Pb as determined by scanning electron microscopy–electron diffraction spectroscopy (SEM–EDX), were used for this study. Batch dissolution experiments of arsenopyrite (1 g L^{-1}) in the presence of 200 μM DFO-B at initial pH (pH_0) 5 were conducted for 110 h. In the presence of DFO-B, release of Fe, As, and Pb showed positive trends with time; less dependency was observed for the release of Fe, As, and Pb in the presence of only water under similar experimental conditions. Detected concentrations of soluble Fe, As, and Pb in suspensions containing only water were found to be *ca.* 0.09 ± 0.004, 0.15 ± 0.003, and 0.01 ± 0.01 ppm, respectively. In contrast, concentrations of soluble Fe, As, and Pb in suspensions containing DFO-B were found to be 0.4 ± 0.006, 0.27 ± 0.009, and 0.14 ± 0.005 ppm, respectively. Notably, the effectiveness of DFO-B for releasing Pb was *ca.* 10 times higher than that for releasing Fe. These results cannot be accounted for by thermodynamic considerations, namely, by size-to-charge ratio considerations of metal complexation by DFO-B. As determined by SEM–EDX, elemental sample enrichment analysis supports the idea that the Fe–S subunit bond energy is limiting for Fe release. Likely, the mechanism(s) of dissolution for Pb incrustations is independent and occurs concurrently to that for Fe and As. Our results show that dissolution of arsenopyrite leads to precipitation of elemental sulfur, and is consistent with a non-enzymatic mineral dissolution pathway. Finally, speciation analyses for As indicate variability in the As(III)/As(V) ratio with time, regardless of the presence of DFO-B or water. At reaction times <30 h, As(V) concentrations were found to be 50–70%, regardless of the presence of DFO-B. These results are interpreted to indicate that transformations of As are not imposed by ligand-mediated mechanisms. Experiments were also conducted to study the dissolution behavior of galena (PbS) in the presence of 200 μM at pH_0 5. Results show that, unlike arsenopyrite, the dissolution behavior of galena shows coupled increases in pH with decreases in metal solubility at $t > 80$ h. Oxidative dissolution mechanisms conveying sulfur oxidation bring about the production of $\{H^+\}$. However, dissolution data trends for arsenopyrite and galena indicate $\{H^+\}$ consumption. It is plausible that the formation of Pb species is dependent on $\{H^+\}$ and $\{OH^-\}$, namely, stable surface hydroxyl complexes of the form $Pb_4(OH)_4^{4+}$ (pH_{50} 5.8) and $Pb_6(OH)_8^{4+}$ for pH values 5.8 or above.

* Corresponding author. Fax: +52 (5) 5616 2145.
E-mail address: jcervini@igg.unam.mx (J. Cervini-Silva).

0016-7037/$ - see front matter © 2008 Elsevier Ltd. All rights reserved.
doi:10.1016/j.gca.2008.02.008

1. INTRODUCTION

Arsenic (As) is widely distributed in nature (*ca.* 5×10^{-4}% earth's crust) (Voigt et al., 1996; Plant et al., 2005). Human beings are exposed to arsenic through food, water, and air. Depending on the route of exposure, inorganic arsenic brings about various health effects including stomach, intestine, and lung irritation, and skin damage. Ingestion of contaminated water containing inorganic arsenic can lead to cancer development, especially in the skin, lungs, liver, or bladder (Pinto and Nelson, 1976; Chen et al., 1985; Smith et al., 2002), and can contribute to a depletion in the production of red and white blood cells.

In geological environments, arsenic can occur in the 5^+, 3^+, 0, 1^-, and 2^- oxidation states (Greenwood and Earnshaw, 1984). Mineral sources of arsenic include *arsenates* [containing As(V)O_4 units] (e.g., adelite [$CaMgAsO_4(OH)$], chalcophyllite [$Cu_{18}Al_2(AsO_4)_3(SO_4)_3(OH)_{27}{\cdot}3^3H_2O$]); *arsenites* [containing As(III)O_3 units] (e.g., armangite [$Mn_{26}(As_{18}O_{50})(OH)_4CO_3$], ecdemite [$Pb_6As_2O_7Cl_4$]); *elemental arsenic* [As(0)], *sulfides and arsenites* (e.g., arsenopyrite [FeAsS], lautite [CuAsS], skutterudite [(Cu, Ni)As_3]), and *sulfosalts* (e.g., orpiment [As_2S_3], realgar [AsS]) (Brown et al., 1999). In addition, arsenic can also be found as a minor or trace component in minerals (e.g., jarosite [$KFe_3(SO_4)_2(OH)_6$]). Arsenic is often found on rock surfaces combined with sulfur or metals, and arsenopyrite and orpiment are the earth's primary mineral sources of As.

The biogeochemical cycling of As is complex, driven by both natural processes such as mineral weathering (Nordstrom and Archer, 2003) and atmospheric deposition, and anthropogenic activities (Merian, 1991). High concentrations of As detected in geographical areas with no documented natural sources reveal the growing contribution of anthropogenic activities to the distribution of As (Nordstrom and Archer, 2003; O'Day et al., 2005). To add to the complexity, the mobility and toxicity of As-bearing compounds vary with As oxidation state. For instance, As either as As(III) or As(V) forms anionic species when in aqueous solution, adsorbed to mineral surfaces, or incorporated into precipitates (Brown et al., 1999), yet As(V) adsorbs more strongly to mineral surfaces than does As(III), and thus is generally less mobile and potentially less bioavailable (Frost and Griffin, 1977; Korte and Fernando, 1991). In contrast, As(III)-bearing compounds are two to three times more toxic than As(V)-bearing compounds (Bottomley, 1984; Ng et al., 2003; Rodríguez et al., 2003), while reduced, inorganic As found in sulfide minerals is relatively low in toxicity. Oxidized inorganic As, either as As(III) or As(V) compounds, are significantly more toxic than many As organic complexes.

Of particular interest for this study is the observation that biological activity instigates arsenopyrite dissolution. For example, incubations of arsenopyrite with *Thiobacillus ferrooxidans* under oxic conditions lead to the solubilization of Fe(III), As(III), and As(V) (Monroy-Fernandez et al., 1995) coupled with the formation of ferric arsenates and elemental sulfur. Comparable As and Fe release values were reported in arsenopyrite samples where bacterial attachment occurs and where it does not. These results hint at the idea that bacterial attachment may not be limiting for mineral dissolution, and that it could also occur because of non-enzymatic pathways, possibly mediated by biogenic compounds such as organic ligands.

Organic ligands of small size and low molecular mass commonly found in soils, such as oxalate, enhance the dissolution of iron minerals (Cornell and Schwertmann, 2003). How organic ligands influence arsenopyrite dissolution remains largely unknown. To the authors' knowledge, there has been little mechanistic work designed to study the non-enzymatic dissolution behavior of mineral arsenic. At circumneutral pH and 25 °C, orpiment and realgar undergo oxidative dissolution (where dissolved oxygen serves as an oxidant) (Lengke and Tempel, 2002), involving the partial oxidation of structural arsenic and sulfur coupled with the formation of arsenates. The predominant As species in solution were arsenates as well as various sulfur species. Another study conducted in the Macraes (Craw et al., 2003) processing plant reports the oxidative dissolution of arsenopyrite. Observed concentrations of soluble As after exposure of arsenopyrite samples to oxidation and agitation for seven days were reported to be *ca.* 580 ppm in unsealed containers and *ca.* 140 ppm in sealed containers. Mineral dissolution was coupled with the precipitation of iron (hydr)oxides (Craw and Pacheco, 2002).

In oxic environments, such as highly weathered soils or surficial seawater, microorganisms and higher plants produce biogenic ligands such as siderophores to mobilize Fe that otherwise would be unavailable (Watteau and Berthelin, 1994; Hersman et al., 1995; Liermann et al., 2000; Maurice et al., 2000; Maurice et al., 2001; Cocozza et al., 2002; Cervini-Silva and Sposito, 2002; Cheah et al., 2003; Kraemer et al., 2005; Haack et al., 2006). Siderophore ligands can facilitate the dissolution of natural particles that represent a primary reservoir of iron, namely, oxide minerals and phyllosilicates including hematite (Hersman et al., 1995), hornblende (Liermann et al., 2000), unsubstituted (Cervini-Silva and Sposito, 2002; Cocozza et al., 2002; Kraemer et al., 2005) or aluminum (Watteau and Berthelin, 1994; Maurice et al., 2000; Cheah et al., 2003) goethite, and kaolinite (Maurice et al., 2001) or smectite (Haack et al., 2006) clay minerals.

Little quantitative information exists, however, on the dissolution of As-bearing minerals in the presence of siderophore ligands. In pioneering experiments with unsubstituted goethite, Watteau and Berthelin (1994) demonstrated the remarkable efficacy of the common trihydroxamate siderophore, desferrioxamine-B (DFO-B), in promoting the solubilization of Fe, as compared to either protons or other common biological ligands such as oxalate. They attributed this difference to the Fe(III)-specific complexing ability of the siderophore ligands. Similarly, Kraemer et al. (2005) reported an enhanced rate of Fe release from goethite in the presence of DFO-B, concluding that coordination of the siderophore to an Fe(III) center at the mineral surface is a precursor to the dissolution process. This mechanistic step was also suggested by Holmén and Casey (1996), Holmén et al. (1999), and by Kalinowski et al. (2000) in their studies of the kinetics of hydroxamate-promoted mineral dissolution. The objective of this study is to investigate the dissolution behavior of arsenopyrite in the presence of DFO-B at pH 5.

2. MATERIALS AND METHODS

2.1. Materials

Specimens of arsenopyrite were extracted from mines in Panasqueira, Portugal, and purchased from Ward's Natural Science Establishment, Inc. Specimens of galena were obtained as gifts from the Mineralogical Collection of the Museum of Geology, Universidad Nacional Autónoma de México.

Prior to use, the mineral samples were prewashed with 6 N HCl, ground in an agate mortar, and sieved. Arsenopyrite samples with particle sizes between 100 and 149 μm were used for this study. Weathering reports of AsSFe have been conducted using AsSFe samples between 50 and 80 μm pre washed with 6 N HCl (Monroy-Fernandez et al., 1995). We selected AsSFe samples with sizes between 100 and 149 μm. We observed in preliminary experiments that AsSFe samples of certain particle sizes would suspend in solution and stick to the vial water and cap, which contributes to mass losses and therefore introduces error for quantifying metal release.

Determinations of specific surface area values were performed by the static BET method. Experiments were conducted in triplicate.

Deionized water produced in a Barnstead Nanopure 4741 system (Iowa, USA; 17.7 MΩ cm) was used in all experiments. Containers and glassware were soaked overnight in 10% (v/v) nitric acid, then washed three times and rinsed with deionized water prior to use. All chemicals were analytical grade.

Desferrioxamine-B mesylate salt [$C_{25}H_{46}N_5O_8NH_3^+(CH_3SO_3^-)$] was purchased from Sigma–Aldrich (Italy). Sodium hydroxide pellets, hydrochloric acid 36.5–38%, potassium iodide granular, nitric acid 70% and sodium borohydride 98% were purchased from Mallinckrodt Baker (USA). Calibrations for atomic absorption spectrometric determinations were performed using commercial 1000 mg L^{-1} arsenic, iron, and lead aqueous solutions purchased from Merck KGaA (Darmstadt, Germany).

2.2. SEM–EDX analyses

Arsenopyrite samples were reacted with 2 mM DFO-B at initial pH 5 for 95 and 430 h, stirred at 150 rpm. Surface analyses were obtained using scanning electron microscopy. Chemical composition analyses of arsenopyrite samples were performed by energy dispersive spectroscopy, using a Cambridge-Leica Stereoscan 440 Scanning Electron Microscope equipped with an Oxford, model Pentafet (EDX). Backscattering electron micrographs were collected for all samples.

2.3. Dissolution experiments

Specimens of arsenopyrite were washed with 6 N HCl prior to use. The dissolution behavior of arsenopyrite was studied in the presence of (I) 200 μM DFO-B solution and (II) water (blank). The initial pH (pH_0) for experimental conditions (I) and (II) was adjusted to 5 by adding aliquots of 0.01 N HCl solutions. Samples were placed in 4-mL Wheaton-sample vials and placed in a stirrer (Orbital Lab-Line Instruments model 4690) at 150 rpm. All experiments were conducted in triplicate. Mineral suspensions were analyzed at various time intervals. Similar experiments were conducted to study the dissolution behavior of galena (PbS).

2.4. Adsorption experiments

Adsorption of DFO-B on arsenopyrite was investigated in batch mode at pH_0 5 with samples open to the atmosphere at room temperature. Specimens of arsenopyrite were placed in 4-mL Wheaton-sample vials. Aliquots of DFO-B stock solutions were then added to achieve the desired solution composition. The total volume of each sample was 4 mL, and the solids concentration adjusted to 1 g L^{-1}. Mineral suspensions were equilibrated for 110 h at 150 rpm, then decanted. Aliquots of the supernatant solution were separated using a 22 G × 32 mm BD syringe needle.

The surface excess of DFO-B was calculated by dividing the concentration loss (initial concentration minus the total ligand concentration in the filtrate) by the solids concentration. Errors in adsorbed concentration were estimated based on equating the sample coefficient of variation to the square root of the sum of squares of the coefficients of variation of the constituent quantities in the definition of the surface excess.

2.5. Analytical techniques

Determinations for DFO-B concentration were conducted using a colorimetric method (Solinas, 1994) using a UV/Vis spectrophotometer (Varian, model Cary 3E) (CA, USA). Samples were acidified with 6 M HCl (*ca.* 1 μL per sample) prior to analysis. The pH values for all samples were 1.5–1.7. Colorimetric determinations were conducted 2 h after adding Fe(III) excess. Spectral deconvolution for the determination of Fe–DFO-B concentration was determined using the minimum squared method for data acquired at $\lambda_{max} = 434$ nm in the presence of Fe(III) excess (as $FeCl_3{\cdot}6H_2O$; Solinas, 1994).

2.6. Determination of total soluble As, Fe, and Pb

Determinations of total soluble As were conducted using an atomic absorption spectrometer/AAS (Varian, SpectrAA 110, Melbourne, Australia) equipped with a hydride generator (HG, Varian, VGA 77) at 193.7 nm. Hydride generation was accomplished by mixing 8 M HCl and 0.6% $NaBH_4$ dissolved in 0.5% NaOH. Reduction of total As to As(III) in the standard or sample solutions was achieved by adding KI as described elsewhere (Elrick and Horowitz, 1986; Moffett, 1988). Experiments were conducted in triplicate. Negative blanks, internal standards, and certified materials were used in all experiments. The experimental detection limit for As was 0.25 ppb. The precision of the measurements was found to be within 0.5–1.5% RSD.

Determinations of total soluble Fe and Pb were conducted by atomic absorption spectrometry using a Varian, SpectrAA 110 equipped with an acetylene-air oxidant flame (AAS-F) at 248.3 and 217.0 nm, respectively. Experimental detection limits were found to be 0.02 for Fe and 0.033 mg L^{-1} for Pb.

2.7. Arsenic speciation

Speciation of As, namely As(III) and As(V), was conducted using an HPLC-AAS method described elsewhere (Georgiadis et al., 2006). Briefly, separation of As(III) and As(V) was conducted using an HPLC (Solvent Delivery System 9012, Varian, CA, USA) with a 100-μL injection loop for sample introduction. This HPLC system was coupled with an AAS (SpectrAA 110, Varian, Mulgrave, Victoria, Australia). The mobile phase consisted of 1.5 mM phosphate at pH 5.8. The mobile phase was pumped isocratically at 2 mL min^{-1} through an analytical anion exchange column (Supelcosil LC-SAX-1 Bellefonte, PA, USA). Trace metal grade 10 M hydrochloric acid and a 0.6%, w/v sodium borohydride solution were pumped at 1 mL min^{-1} to generate arsine gas. The arsine gas was detected by AAS-F.

3. RESULTS AND DISCUSSION

3.1. Surface area determination

Walker et al. (2006) conducted surface area measurements for arsenopyrite (177–250 μm) using a NOVA Quantachrome 1000 equipped with nitrogen adsorption. The average specific surface area was reported to be 0.0388 $m^2\ g^{-1}$. Experimental determinations of specific surface area values using the static BET method were found to be statistically not different from zero with a high degree of uncertainty. We infer that the arsenopyrite particles used in this study are more soluble than arsenopyrite samples used elsewhere (Walker et al., 2006) because the interfacial energy (γ) is a positive contribution to the total energy according to the equation:

$$\log K_{sp}{}' = \log K_{sp}{}^{BULK} + \frac{2/3\gamma}{2.3RT}S \quad (1)$$

where $K_{sp}{}'$ is the conditional solubility product, $K_{sp}{}^{BULK}$ is the solubility product of the bulk material, S is the surface area per mole, $R = 8.314$ J mol^{-1} K, and T is the temperature in K (Stumm and Morgan, 1996). Limited predictions using Eq. (1), however, are to be considered because it assumes that γ is not itself size dependent (Zhang et al., 1999). Also, accurate γ measurements are commonly unavailable, particularly for hydrated surfaces that may be coated with organic ligands.

An exercise to estimate the surface area of the arsenopyrite specimen used in this study was conducted using a geometrical estimation based on particle size and shape. Calculations of the specific surface area (S_{sa}) of 100–149 μm (D) arsenopyrite were conducted assuming a spherical shape for all particles and a density for arsenopyrite (ρ) of 6.09–6.17 g cm^{-3}, and according to:

$$S_{sa} = \frac{6}{D\rho} \quad (2)$$

S_{sa} values were found to be in the range 0.0065–0.00985 $m^2\ g^{-1}$. For the purpose of comparison, similar estimates using Eq. (2) for arsenopyrite samples reported to have 0.0388 $m^2\ g^{-1}$, as determined by the BET method (Walker et al., 2006), were found to be in the range 0.0038–0.00558 $m^2\ g^{-1}$. Experimental and theoretical surface area determinations differ by a factor of 10 or more. Therefore, no attempts to use estimated surface area values to calculate dissolution rates normalized to surface area were conducted. Metal release values are referred to the initial mass of the mineral sample.

3.2. SEM–EDX analyses

Experiments to study surface morphology using arsenopyrite crystal samples were conducted. Results are shown in Fig. 1a–e.

Arsenopyrite samples were exposed to (I) water only or (II) a 2 mM DFO-B solution. Solid samples were studied after 95 and 430 h of reaction time. Micrographs of arsenopyrite without treatment show the presence of lead (Fig. 1a). EDX analyses confirm that the lead is in the elemental form (Fig. 2). The darker coloration is attributed to a higher Fe content.

Analyses show incrustations of elemental Pb in all arsenopyrite samples, regardless of treatment. Our results contrast with the well-known association of arsenopyrite with sulfide minerals, namely galena (PbS), pyrrhotite ($Fe_{1-x}S$) ($x = 0$–0.2), pyrite (FeS_2) or chalcopyrite ($CuFeS_2$), sphalerite (ZnS), molybdenite (MoS_2), and others (e.g., Palache et al., 1944). In nature, arsenopyrite is also known to be found in association with gold (Au), bismuth (Bi), and Sn minerals. We hypothesize that the presence of incrustations of elemental Pb can be explained, in part, because highly reducing conditions prevailed during rock formation.

Fig. 1b shows arsenopyrite samples exposed to water after 95 h of reaction time. Our results indicate the presence, *albeit* scattered, of small-sized arsenopyrite particles, while dissolution patterns or signs of surface attack are scarcely found. Well-defined borders and growth patterns denote surface crystallinity.

Fig. 1e shows AsSFe exposed to water for 430 h. Well-defined growth lines are still evident. This is not the case for arsenopyrite samples exposed to 2 mM DFO-B for 95 h (Fig. 1c and d). Micrographs clearly show signatures of mineral dissolution and denote ubiquitous small-sized particles, possibly due to energy lattice disruption and fragmentation. On the other hand, incrustations of elemental Pb show strong attack signatures in the presence of DFO-B (Fig. 1d). It is worth noting that dissolution effects become more pronounced upon exposure to DFO-B, as compared to water only. Fig. 1d depicts thin erosion lines throughout the mineral surface and fractures, and also depicts Pb incrustations with evidence of erosion throughout the mineral surface. The more extensive weathering of Pb could be interpreted to mean faster dissolution kinetics associated with the former than with the latter.

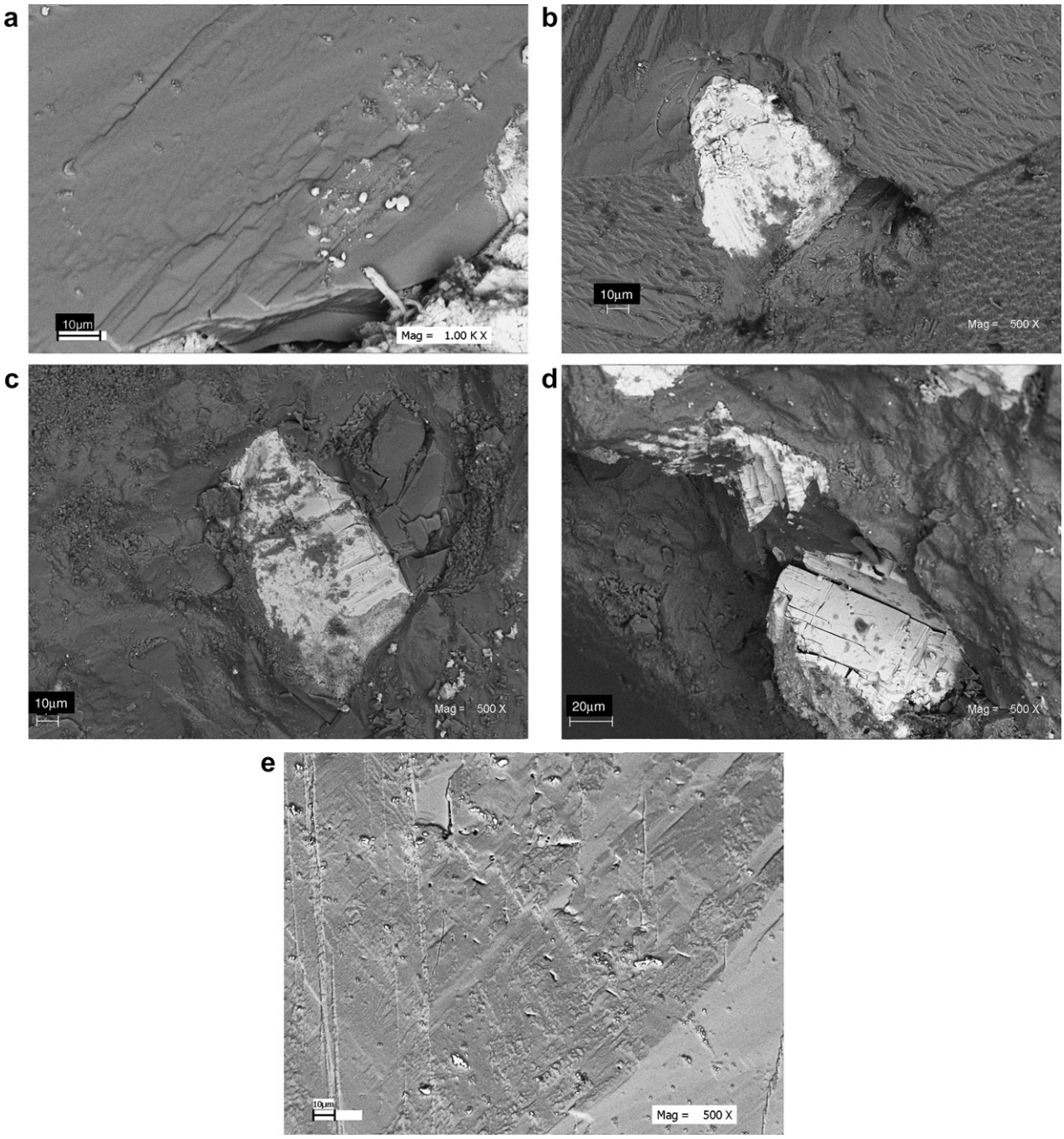

Fig. 1. Scanning electron micrographs of arsenopyrite crystals. Arsenopyrite samples were exposed to (I) water only or (II) a 2-mM DFO-B solution. Solid samples were studied after 95 and 430 h of reaction time. (a) The presence of elemental lead (see Fig. 2 for the corresponding EDX analysis). (b) Arsenopyrite crystals after 95 h exposure to water at pH 5. (c and d) Arsenopyrite crystals after 95 h exposure to 2 mM DFO-B at pH 5. (e) Arsenopyrite crystals after >430 h exposure to water.

Data listed in Table 1 show elemental analyses of arsenopyrite crystal samples exposed to varying solution compositions at $t = 95$ and 430 h. As evidenced by S surface enrichment with corresponding data for Fe and As release (Figs. 3 and 4), the following observations can be drawn.

Samples exposed to 2 mM DFO-B show comparable amounts of structural Fe relative to samples exposed to water only. These observations contrast with solution composition data (Fig. 3), and are consistent with mineral dissolution. In contrast, samples exposed to 2 mM DFO-B show enrichment in As relative to those samples exposed to water only, and are consistent with trends in As release (Fig. 4). Likely, the mechanisms for Fe and As release are independent of the solution chemical composition, and from each other.

Arsenopyrite samples exposed to 2 mM DFO-B show enrichment in S relative to those samples exposed to water only (Table 1). These findings agree well with reports of

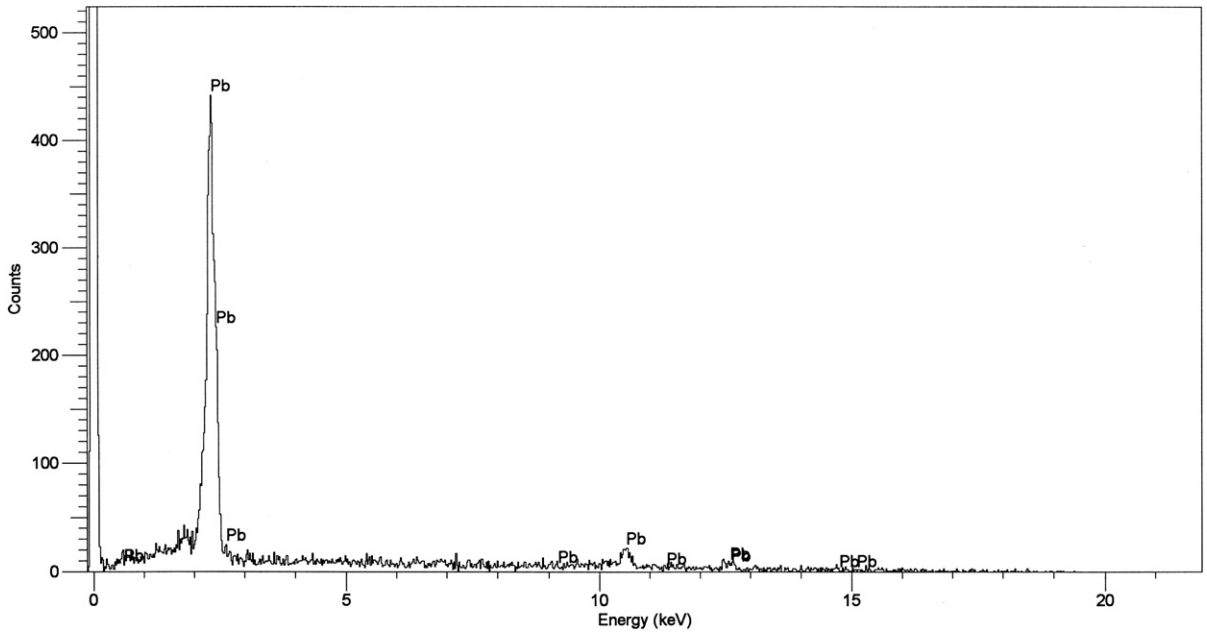

Fig. 2. EDX Analysis for arsenopyrite surfaces and the presence of elemental Pb.

Table 1
EDX analyses of arsenopyrite crystals exposed to aqueous solutions of 2 mM DFO-B at pH_0 5

	% Atomic weight					
	Fe	As	S	Fe	As	S
	No treatment					
	31.8 ± 2.8	33.1 ± 2.2	35.1 ± 0.7			
	Water			200 mM DFO-B		
Time (h)						
95	34.6 ± 1.9	32.9 ± 1.3	32.5 ± 0.5	32.8 ± 0.7	31.7 ± 1.4	35.5 ± 2.1
432	31.9 ± 1.9	34.9 ± 0.5	33.2 ± 1.4	30.6 ± 0.9	33.7 ± 1.1	35.7 ± 6

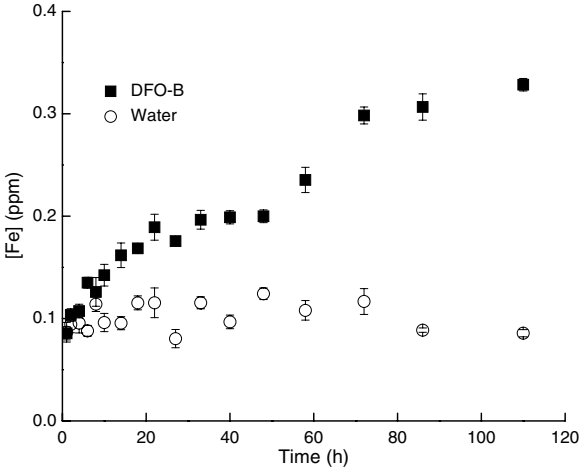

Fig. 3. Release of Fe after reacting arsenopyrite (0.149–0.1 mm) with (a) water (closed circles) and (b) 200 μM DFO-B (closed squares) at pH_0 5.

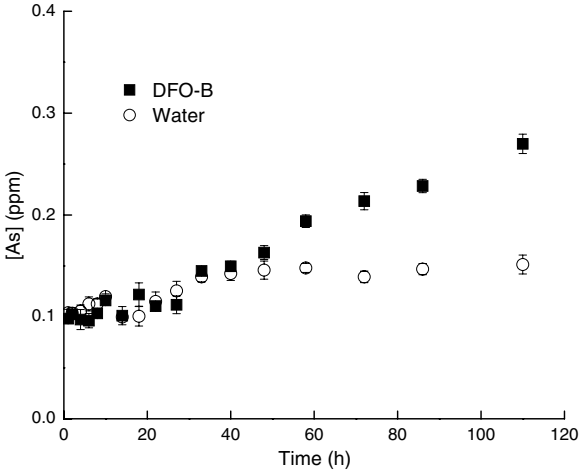

Fig. 4. Release of As after reacting arsenopyrite (0.149–0.1 mm) with (a) water (open circles) and (b) 200 μM DFO-B (closed squares) at pH_0 5.

elemental sulfur deposition on AsSFe (Steudel, 1996; Cruz et al., 1997; Rohwerder et al., 2003). Voltammetric and XRD studies of the biogenic dissolution of arsenopyrite report that the precipitation of elemental sulfur occurs as a consequence of abiotic and biotic mechanisms (Rohwerder et al., 2003). In the former case, the authors attribute elemental sulfur precipitation to Fe^{3+} ions that induce the formation of passive layering according to the reaction:

$$FeAsS + 7Fe^{3+} + 4H_2O \rightarrow H_3AsO_4 + 8Fe^{2+} + S^0 + 5H^+ \quad (3)$$

The precipitation of elemental sulfur can also occur as a consequence of arsenopyrite oxidation in the presence of *T. ferrooxidans* according to the reaction:

$$FeAsS + 8Fe^{3+} + (4+n)H_2O \rightarrow FeAsO_4(nH_2O) + 8Fe^{2+} + S^0_{(surface)} + 8H^+ \quad (4)$$

The formation of elemental sulfur has been explained as being due to the oxidation of aqueous sulfur species in the presence of transition metals, including Fe(III) at slightly acidic pH (Steudel, 1996). Metal sulfides such as sphalerite, galena, arsenopyrite, chalcopyrite, and hauerite (ZnS, PbS, FeAsS, $CuFeS_2$, and MnS_2, respectively) dissolve through both electron extraction by iron(III) ions and proton attack (Rohwerder et al., 2003). In the absence of iron(III) ions, bacteria oxidize free sulfide (H_2S) resulting from the proton attack on the metal sulfide via elemental sulfur to sulfuric acid. Such a reaction mechanism entails the regeneration of protons previously consumed because metal sulfide dissolution.

3.3. Variations of pH

Fig. 5 shows the variation of pH in the supernatant solution of arsenopyrite suspensions exposed to water or DFO-B. Our results show the positive variations in pH resulting from long-term reaction of arsenopyrite. This is particularly true in the case of water. Decreases in pH values are observed only within the first 4 h of reaction time. A progressive increase in pH values is recorded within 30 h reaction time, regardless of solution composition. Steady changes in pH values occurred for $t > 30$ h. The more quantitative changes of pH observed in the absence of DFO-B can be explained in part due to DFO-B acid–base equilibria in suspension. At time $t = 0$, DFO-B is mostly present as DFO-B^+. After 4 h, decreases in [DFO-B^+] were coupled with increases in DFO-B, while the pH value approached that of the pK_a for the DFO-B^+/DFO-B acid–base pair, 8.1 (Telford and Raymond, 1996). These observations are consistent with the idea that the DFO-B acid–base pair could be serving as a buffer.

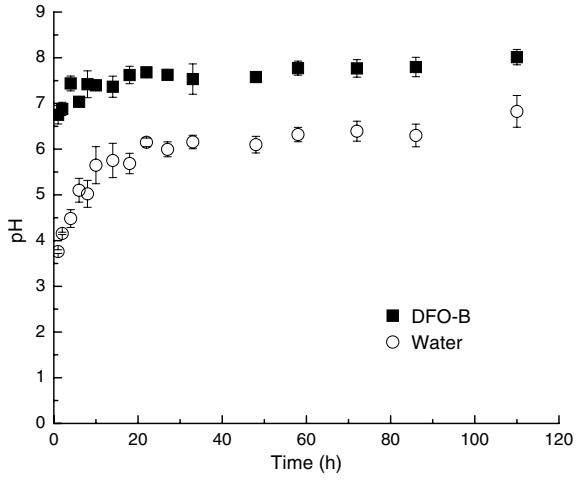

Fig. 5. Variations of pH during the reaction between 1 g L^{-1} arsenopyrite and 200 μM DFO-B.

Data in Fig. 5 indicate that variations in proton activity did not have an effect on the release of As after reacting arsenopyrite at $t < 30$ h, regardless of the presence of DFO-B. Furthermore, the amounts of Fe found in suspensions containing DFO-B at $t < 30$ h were found to surpass those found in the presence of water only. The effect of DFO-B on Fe release became evident within the first hours of reaction time. It follows that ligand-promoted dissolution dominates over proton-promoted dissolution in spite of the fact that the recorded pH values were found to be lowest at $t < 30$ h.

It is worth noting that variations in pH following arsenopyrite dissolution in the presence of DFO-B or water only contrast with a report (Rohwerder et al., 2003) on increases in proton activity following biogenic dissolution of arsenopyrite as described by Eqs. (3) and (4), and are inconsistent with independent mineral dissolution mechanisms.

3.4. Release of Fe, As, and Pb

Our results show that following exposure of arsenopyrite (100–149 μm, 1 g L^{-1}) to water at pH 5 after 5 days, total soluble As can be as high as 0.15 ppm. Thus, arsenopyrite specimens were prewashed prior to use. Fig. 3 shows the amounts of dissolved Fe following the reaction of arsenopyrite with water or DFO-B containing solutions at pH 5. In the presence of water, variations in Fe are negligible even after 110 h of reaction time. In the presence of DFO-B, however, releases of Fe increase with time. These results coincide with observed decreases in % Fe in arsenopyrite samples exposed to similar reaction conditions (Table 1). This is particularly the case at longer reaction times.

Fig. 4 shows the effect of 200 μM DFO-B on the dissolution behavior of mineral As. At reaction times <40 h, the presence of DFO-B on mineral dissolution was found to have a negligible effect. The effect of DFO-B on mineral dissolution became evident at longer reaction times. After 110 h, the dissolution of As in the presence of water only and DFO-B corresponded to 0.151 ± 0.003 and 0.270 ± 0.009 ppm of As, respectively.

Fig. 6 summarizes data pertinent to the extent of As, Fe, and Pb release with time. At reaction times surpassing 110 h, dissolved Fe and As values were found to be as high as 0.328 ± 0.006 and 0.270 ± 0.009 ppm, respectively. Our results can be explained because a non-conservative mineral dissolution pathway. In the presence of DFO-B, the con-

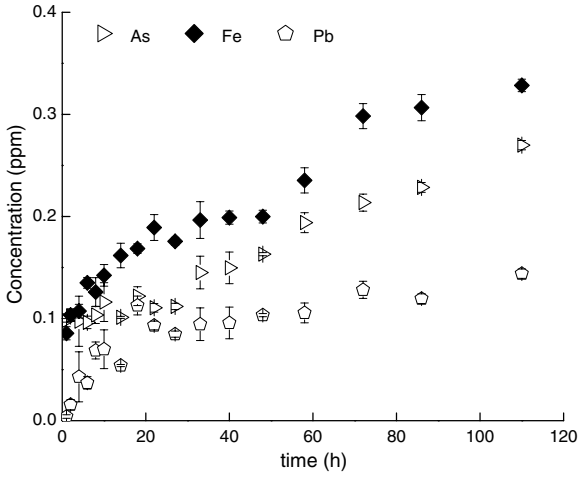

Fig. 6. Comparison between the release of As (open triangles), Fe (closed rhomboids), and Pb (open pentagons) after reacting arsenopyrite (0.149–0.1 mm) with 200 μM DFO-B at pH_0 5.

centration of soluble Pb was found to be *ca.* 0.144 ± 0.005 ppm. In contrast, in the presence of water only, the concentration of soluble Pb was found to be below the analytical detection limits (<0.05 ppm).

3.5. Elemental analyses

Arsenopyrite samples were digested in acid (25 g L^{-1}; 0.5 g arsenopyrite in 20 mL HNO_3 70%) for 5 days. Brownish vapors were liberated and a yellowish precipitate formed within the first hours of reaction time. These results agree well with reports of releases of sulfur oxides and the formation of elemental sulfur following enzymatic pathways for arsenopyrite dissolution (Rohwerder et al., 2003). Notably, data trends for S sample enrichment parallel that for Fe (Table 1), which could be an indication that the bond energy of Fe–S subunits limits Fe release.

Fig. 7 shows the dissolution behavior of Fe, As, and Pb. *Y*-axis units, % dissolved, correspond to the concentrations of As, Fe, and Pb divided by the total concentrations of As, Fe, and Pb, respectively, 100×. Total concentrations of As, Fe, and Pb were determined by acid digestion. Chemical analyses following acid digestion of arsenopyrite samples (25 g L^{-1}) in 70% nitric acid showed total soluble As, Fe, and Pb to be *ca.* 13,950, 13,417, and 434 ppm, respectively. Therefore, total concentrations of Pb, As, and Fe following exposure of 1 g L^{-1} arsenopyrite to either DFO-B or water only were not expected to surpass 17.4, 558, and 537 ppm, respectively. Maximum detected concentrations (after 110 h reaction time) of Pb, As, and Fe were ⩽0.15 ppm (*ca.* 1% total Pb), ⩽0.27 ppm (0.05% of the total As), and *ca.* 0.328 ppm (0.06% total Fe), respectively. While on a molar basis the effectiveness of DFO-B for releasing Fe and As is comparable, the effectiveness of DFO-B for releasing Pb is 10 times that for releasing either Fe or As. These kinetic observations for the release of Pb cannot be accounted for by thermodynamic considerations for metal complexation by DFO-B alone (Hernlem et al., 1999).

3.6. As speciation

Listed in Table 2 are data pertinent to the speciation of As after reacting arsenopyrite (100–149 μm) with (a) water (closed circles) and (b) 200 μM DFO-B (closed squares) at pH_0 5. In both scenarios, there are variations in the As(III)/As(V) ratio with time. At reaction times <30 h, concentrations of As(V) were found to be as high as 50–70%, regardless of the presence of DFO-B. At longer reaction times, $30 < t < 120$ h, however, As undergoes reduction from As(V) to As(III). As(III) becomes the predominant As species in solution (Table 2) with no concomitant variations in pH (Fig. 5). It follows that the reduction of As(III) cannot be accounted for by evidence of sulfur oxidation alone (Table 1). The lack of variation in proton activity following fluctuations in As speciation (arguably due to sulfur oxidation) serves as an indication that mechanisms other than Eqs. (3) or (4) prevail in suspension.

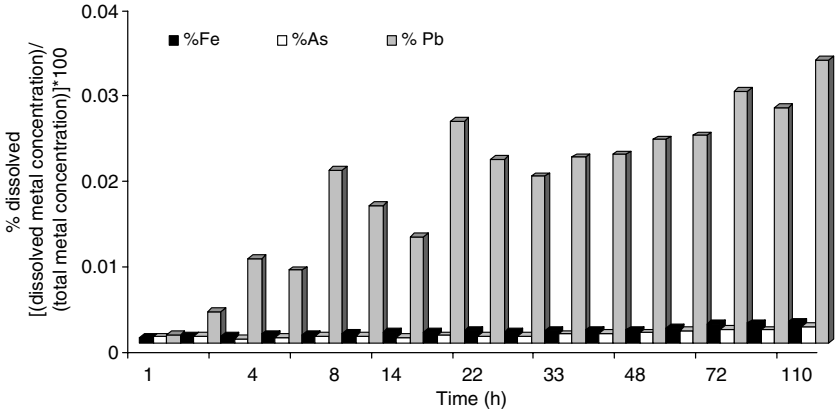

Fig. 7. Molar comparison between the release of As, Fe, and Pb after reacting arsenopyrite (0.149–0.1 mm) with 200 μM DFO-B at pH_0 5. The *y*-axis units, % dissolved, correspond to the concentrations of As, Fe, and Pb divided by the total concentrations of As, Fe, and Pb, respectively, 100×. Total concentrations of As, Fe, and Pb were determined by acid digestion.

Table 2
Speciation of As after the Reaction between Arsenopyrite and 200 μM DFO-B at pH_0 5

Time (h)	Water			200 μM DFO-B		
	% As total		As total	% As total		As total
	As(III)	As(V)	(ppm)	As(III)	As(V)	(ppm)
0	98.4 ± 0.4	1.64 ± 0.4	0.04 ± 0.01	99.4 ± 0.3	0.6 ± 0.3	0.03
4	52.4 ± 8.5	47.5 ± 4.5	0.1 ± 0.01	35.9 ± 11.5	64.1 ± 11.5	0.15 ± 0.07
27	28.9 ± 7.4	71.1 ± 7.4	0.5 ± 0.04	43.2 ± 10.4	56.8 ± 10.4	0.6 ± 0.05
58	78.1 ± 4.2	21.9 ± 4.2	0.5 ± 0.07	94.2 ± 4.2	5.8 ± 4.25	0.65 ± 0.07
110	96 ± 7.6	4.01 ± 0.60	0.5 ± 0.05	81.6 ± 7.6	18.4 ± 7.6	1.10 ± 0.09

3.7. Arsenic speciation and dissolved oxygen concentration

Fig. 8 shows data trends pertinent to dissolved oxygen concentrations in arsenopyrite suspensions in the presence of DFO-B or water only. The dissolved oxygen concentration varies with solution composition.

In the presence of water and at $t = 3$ h of reaction time, there are no decreases in dissolved oxygen concentration [O_2], and there is evidence of As(V) accumulation. For the case of $t = 30$ h, there is little variation of [O_2] coupled with increasing accumulation of As(V), and for the case of $t = 60$ h, our data show decreases in [O_2] coupled with the accumulation of As(III) and the depletion of [As(V)], a signature of suboxic conditions. At longer reaction times ($t = 110$ h), [O_2] increases, albeit slightly, while As(III) accumulates steadily. Taken together, these observations indicate that dissolved molecular oxygen does not serve as the ultimate electron acceptor towards arsenic in an exclusive manner.

The presence of DFO-B in arsenopyrite suspensions affects the speciation of As and dissolved oxygen concentration. Our results show that at short reaction times ($t = 3$ h), there is a sharp depletion of [O_2] coupled with the accumulation of As(V). At longer reaction times ($t = 30$ h) [O_2] increases while the concentrations of As(III) and As(V) remain invariant. These results indicate that [O_2] participates in existing reaction mechanisms in suspension in addition to those controlling As redox cycling. This is further confirmed by the observation that at $t = 60$ h, our data show no variations in [O_2] coupled with the quantitative accumulation of As(III) in solution. We note that there is a lack of variation of Fe(III) as affected by [O_2] at $0 < t < 110$ h. Thus, iron redox cycling does not appear to be controlling speciation of As in suspension. At the same time, fluctuations in the As(III)/As(V) ratio occur at earlier reaction times, $t < 60$ h, as evidenced by the lack of variation in [O_2], [As(III)], and [As(V)] at $t = 120$ h. We note that stabilizing mechanisms for As(III) ought to prevail in suspension for them to outcompete oxidation of As(III) to As(V) by O_2.

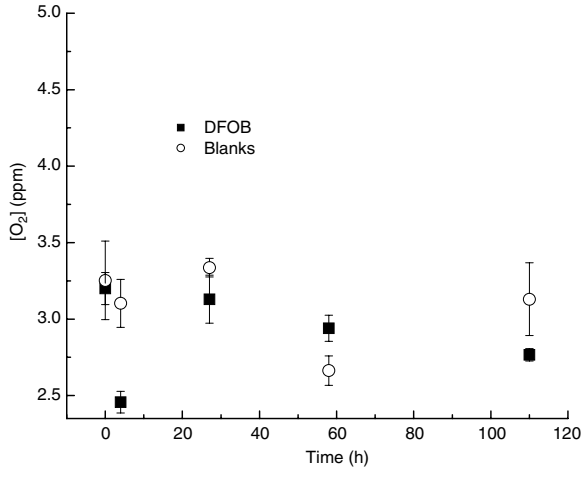

Fig. 8. Dissolved oxygen concentration profiles in arsenopyrite suspensions in the presence of (a) water (open circles) and (b) 200 μM DFO-B (closed squares) pH_0 5. The units of dissolved oxygen concentration are ppm.

Thus far, the data presented herein indicates that DFO-B influences proton exchange reactions which could exert an effect in sulfur speciation (Eqs. (3) and (4)). EDX analyses conducted on arsenopyrite surfaces (Table 1) show higher accumulations of sulfur in samples exposed to DFO-B. These results coincide with observed lower contents of O_2 in arsenopyrite suspensions containing DFO-B (Fig. 8). As discussed above, there is a lack of correlation between As speciation and dissolved oxygen concentration. In this scenario, sulfur speciation becomes pivotal for As redox cycling.

Like orpiment and amorphous As_2S_3, arsenopyrite is thought to undergo oxidative dissolution with the concomitant oxidation of sulfur by dissolved oxygen (Lengke and Tempel, 2002). It has been proposed that as in pyrite oxidative dissolution, sulfur may be predominantly in the form of polythionates following mineral dissolution at circumneutral pH (Goldhaber, 1983; McKibben and Barnes, 1986; Moses et al., 1987). The lifetime of polythionates has been reported (Lengke and Tempel, 2002) as short, arguably due to their quick removal from near the pyrite surface, which acts as catalysts for their oxidation to sulfate. Reportedly, Eqs. (5) and (6) proceeds in an incomplete manner and cannot be accounted for by experimental observations (Lengke and Tempel, 2002):

$$As_2S_3 + 10O_2 + 6H_2O \rightarrow 2HAsO_4^{2-} + 3SO_4^{2-} + 10H^+ \quad (5)$$

$$As_2S_3 + 10O_2 + 6H_2O \rightarrow 2H_2AsO_4^{-} + 3SO_4^{2-} + 8H^+ \quad (6)$$

$$As_2S_3 + 6O_2 + 6H_2O \rightarrow 2HAsO_3 + 3SO_4^{2-} + 6H^+ \quad (7)$$

A related report of PHREEQC calculations (Parkhurst, 1995) indicated that As(III) exists predominantly as H_3AsO_3 (Eq. (7)) and As(V) as $HAsO_4^{2-}$ [Eqs. (5) and

(6)]. However, steady-state dissolution experiments on orpiment oxidation at pH 6.8–8.2 show that the ratio of As(III)/As(V) is 1.1–2.2, regardless of the total As concentration (Lengke and Tempel, 2002). In that study, the rate of orpiment oxidation was found to depend on the concentration of dissolved oxygen content within the range of oxygen concentration studied (6.4–17.4 ppm O_2; Lengke and Tempel, 2002). In that study, it was shown that As(III)/As(V) ratio values following arsenopyrite dissolution (Table 2) can be significantly higher ($t \leqslant 110$ h) than reported As(III)/As(III) values for orpiment (Lengke and Tempel, 2002). Furthermore, our experiments on arsenopyrite dissolution show that there is a lack of correlation between As redox cycling (Table 2) and oxygen concentrations (Fig. 8). Therefore, conjectures on common dissolution mechanisms pathways cannot be withdrawn. Rather, discrepancies between experimental results are interpreted to mean that parallel dissolution pathways of minerals bearing As and S take place. We do not discard the possibility that polythionates may participate in As redox cycling during arsenopyrite dissolution.

3.8. Interaction between DFO-B and arsenopyrite surfaces

The effect of reaction time on the adsorption behavior of DFO-B on the surface of arsenopyrite at pH_0 5 was studied. Our results show small variations of DFO-B concentration after 110 h reaction time and, as a consequence, determinations of DFO-B surface excess values were found to be within error (not shown). These observations suggest that the kinetics for ligand–surface complexation are fast, while those of desorption are slower. A lack of correlation between pH variations at reaction times $t \leqslant 24$ h (Fig. 5) with DFO-B adsorption behavior further indicates that variations in pH have a small effect on the amount of free DFO-B in solution (not associated with the mineral surface).

The poor surface affinity of DFO-B is explained by the small number of adsorption sites (e.g., $a_s \sim 0.0388\ m^2\ g^{-1}$; Walker et al., 2006). In addition, plausible steric hindrance encountered by DFO-B while attempting to complex an Fe(III) center in the mineral may still play a role. Cocozza et al. (2002) hypothesized that both hydrophobic and stereochemical effects limit the siderophore to bind with only one of its three hydroxamate groups for complexing Fe(III) centers.

3.9. Release of structural Pb

To further understand the influence of the presence of Pb in the structure of arsenopyrite on mineral dissolution, experiments were conducted to study the dissolution behavior of galena (PbS) in the presence of 200 μM DFO-B at pH_0 5. Data pertinent to Pb release and pH variations with time are shown in Figs. 9 and 10. As for arsenopyrite, the presence of DFO-B influences the magnitude of gradients in proton concentration. In comparison, for the case of arsenopyrite there is a shallower net gradient in proton concentrations imposed in the presence of DFO-B compared to that of water only (Figs. 5 and 10). For the case of galena in

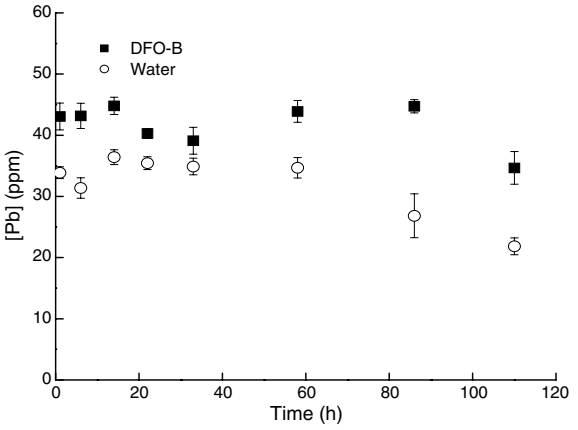

Fig. 9. Release of Pb after reacting galena (0.149–0.1 mm) with (a) water (open circles) and (b) 200 μM DFO-B (closed squares) at pH_0 5.

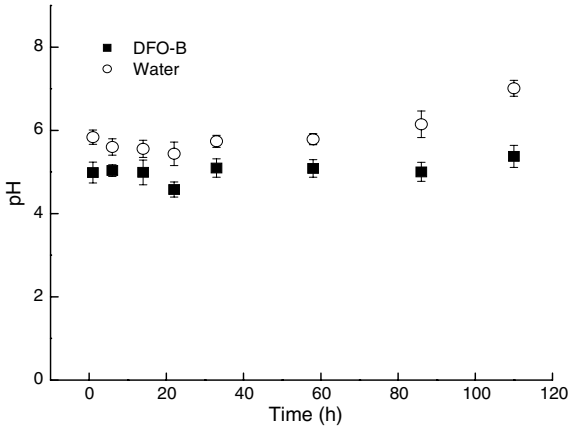

Fig. 10. Variations of pH during the reaction between 1 g L^{-1} galena and 200 μM DFO-B.

the presence of water, variations in proton activity take place at long reaction times ($t > 80$ h). These results contrast with data pertinent to arsenopyrite suspensions in water showing variations in pH at short reaction times, a signature of proton exchange equilibria. In the presence of DFO-B, suspensions containing arsenopyrite or galena, variations in pH in suspensions are still shallow (Fig. 10). These results agree well with the hypothesis that DFO-B acid–base pair can serve as a buffer in suspension. Unlike the dissolution behavior of arsenopyrite (Figs. 3–5), the dissolution behavior of galena shows coupled increases in pH with decreases in metal solubility at $t > 80$ h (Figs. 9 and 10). The consumption of protons and increase in $\{OH^-\}$ activity in suspension holds true, regardless of the presence of DFO-B.

Recent studies (De Giudici et al., 2005, 2007) have reported the dissolution of cleaved (001) galena at $1.2 < pH < 5.8$ under oxic conditions. As determined by fluid-cell micro-Raman Spectroscopy (μRS), following dissolution a layer of several tens to hundreds of nanometers composed of Pb oxides, sulfates, and sulfur metastable spe-

Table 3
Conditional formation constants (K_c) used in model calculations PHREEQC (Parkhurst, 1995) for the system lead and DFO-B in water

	$\log K_c$		$\log K_c$
$DFO^{3-} + H^+ \leftrightarrow HDFO^{2-}$	10.46	$CO_3^{2-} + OH^- + Pb^{2+} \leftrightarrow PbOHCO_3^-$	10.70
$HDFO^{2-} + H^+ \leftrightarrow H_2DFO^-$	9.35	$OH^- + Pb^{2+} \leftrightarrow PbOH^-$	6.58
$H_2DFO^- + H^+ \leftrightarrow H_3DFO$	8.90	$2OH^- + Pb^{2+} \leftrightarrow PbOH_2(aq)$	11.18
$H_3DFO + H^+ \leftrightarrow H_4DFO^+$	8.38	$3OH^- + Pb^{2+} \leftrightarrow PbOH_3^-$	14.23
$HDFO^{2-} + Pb^{2+} \leftrightarrow PbHDFO$	9.48	$OH^- + 2Pb^{2+} \leftrightarrow Pb_2OH^{3+}$	7.61
$H_2DFO^- + Pb^{2+} \leftrightarrow PbH_2DFO^+$	8.99	$4OH^- + 3Pb^{2+} \leftrightarrow Pb_3(OH)_4^{2+}$	32.66
$H_3DFO + Pb^{2+} \leftrightarrow PbH_3DFO^{2+}$	5.92	$4OH^- + 4Pb^{2+} \leftrightarrow Pb_4(OH)_4^{4+}$	36.20
$HDFO^{2-} + 2Pb^{2+} \leftrightarrow Pb_2HDFO^{2+}$	15.77	$8OH^- + 6Pb^{2+} \leftrightarrow Pb_6(OH)_8^{4+}$	69.16
$CO_3^{2-} + Pb^{2+} \leftrightarrow PbCO_3(aq)$	4.56	$CO_3^{2-} + H^+ \leftrightarrow HCO_3^-$	10.46
$2CO_3^{2-} + Pb^{2+} \leftrightarrow Pb(CO_3)_2^{2+}$	8.02	$HCO_3^- + H^+ \leftrightarrow H_2CO_3$	6.402
$CO_3^{2-} \leftrightarrow PbCO_3(s, cerrusite)$	−13.49		

All K_c values are corrected to $I = 0.01$ M. Data as reported in Kraemer et al. (2002), where K_c values were taken from Martell et al. (1995) and Hernlem et al. (1995).

cies forms at the galena surface (De Giudici et al., 2007). Reportedly, galena dissolution rates decrease with pH and reaction time. Our results (Figs. 9 and 10) display similar trends in reactivity after the reaction between galena and DFO-B at pH_0 5. De Giudici et al. (2007) attributed the formation of Pb oxides to partial sulfur oxidation. Arguably, sulfur oxidation occurs at the interface due to reaction with dissolved O_2 with S atoms at the galena surface, or in the immediate vicinity. Subsequently, oxygen combines with Pb ions to form Pb oxide at the interface. We do not discard the notion that small-sized lead oxides form upon dissolution of Pb (Fig. 1b) and dissolving sulfur.

Exposure of different sources of Pb(II)-bearing different initial amounts of structural Pb, namely, arsenopyrite and galena, to 200 μM DFO-B led to the release of *ca.* 1% and 5% total soluble Pb (as determined by acid digestion), respectively. In the former case, DFO-B is present in molar excess relative to Pb. By comparing the amount of Pb released in both scenarios, it is clear that mineral Pb, structural or adsorbed, limits mineral dissolution.

Oxidative dissolution mechanisms conveying sulfur oxidation bring about the production of $\{H^+\}$ (e.g., Nordstrom and Archer, 2003). However, dissolution data trends for arsenopyrite and galena indicate the consumption of $\{H^+\}$ (Figs. 5 and 10). Our results show that the presence of DFO-B affects both variations in proton activity with time and the release of Pb. Thus, it is expected that aside from the formation of Pb oxides (De Giudici et al., 2007), other Pb species dependent on $\{H^+\}$ and $\{OH^-\}$ may be forming in suspension. The authors note speciation considerations reported elsewhere (see Table 3 after Kraemer et al., 1999) and the plausible formation of stable surface hydroxyl complexes of the form $Pb_4(OH)_4^{4+}$ (pH_{50} 5.8) and $Pb_6(OH)_8^{4+}$ for pH values 5.8 or above (Baes and Mesmer, 1976).

4. CONCLUSIONS

In this study, we have reported the dissolution of arsenopyrite and galena (1 g L^{-1}) in the presence of a siderophore ligand (desferrioxamine-B, DFO-B) at pH_0 5 for 140 h. Detected concentrations of soluble Fe, As, and Pb in suspensions containing water only were found to be *ca.* 0.09 ± 0.004, 0.15 ± 0.003, and 0.01 ± 0.01 ppm, correspondingly. In contrast, concentrations of soluble Fe, As, and Pb in suspensions containing DFO-B were found to be 0.4 ± 0.006, 0.27 ± 0.009, and 0.14 ± 0.005 ppm, respectively. Notably, the effectiveness of DFO-B for releasing Pb was almost ten times higher than that for releasing Fe. Our results show that the dissolution of arsenopyrite leads to precipitation of elemental sulfur, and is consistent with a non-enzymatic mineral dissolution pathway. Speciation analyses for As indicate variability in the As(III)/As(V) ratio with time, regardless of the presence of DFO-B or water only. At reaction times $t < 30$ h, As(V) concentrations were found to be 50–70%. This is true regardless of the presence of DFO-B. Hence, redox transformations of As are not accounted for by ligand-mediated mechanisms. This paper provides evidence to show that As speciation, and thus toxicity, following biogenic arsenopyrite dissolution may occur due to non-enzymatic pathways.

Our findings agree well with reports of elemental sulfur deposition on AsSFe (Steudel, 1996; Cruz et al., 1997; Rohwerder et al., 2003) as a consequence of abiotic [Eq. (3)] and biotic mechanisms [Eq. (4)]. On a molar basis, iron release values following weathering of arsenopyrite in the presence of siderophore ligands were found to be much lower than values reported as a consequence of arsenopyrite oxidation in the presence of *T. ferrooxidans* (Monroy-Fernandez et al., 1995). Incubations of 32–53 μm arsenopyrite (20 g L^{-1} suspension) with *T. ferrooxidans* at pH 1.8 under oxic conditions reportedly brings about Fe releases of approximately 100 ppm after 4 d, increasing to 1000 ppm after 30 d (Monroy-Fernandez et al., 1995). Experiments were also conducted to study the dissolution behavior of galena (PbS) (1 g L^-) in the presence of 200 μM DFO-B at pH_0 5. The solubility of galena decreases with pH and time. The consumption of $\{H^+\}$ during the dissolution of galena was explained through the possible formation of stable surface hydroxyl complexes of the form $Pb_4(OH)_4^{4+}$ (pH_{50} 5.8) and $Pb_6(OH)_8^{4+}$ for pH values 5.8 or above.

ACKNOWLEDGMENTS

Hilda Cornejo-Garrido gratefully acknowledges the support of an undergraduate fellowship from The National Autonomous University of Mexico [DGAPA-UNAM, PAPITT (Grant No. IN116007-2)]. Javiera Cervini-Silva thanks the support of the Mexican Academy of Sciences (Academia Mexicana de Ciencias) and The United States-Mexico Foundation for Science (Fundación México-Estados Unidos para la Ciencia) through the 2006-Young Researcher Summer Program Fellowship (AMC-FUMEC). The authors are most grateful to Kent Ross (University of California Berkeley) for providing mineral samples, and to Elizabeth Chávira (Instituto de Investigación en Materiales, UNAM), Sergey Sedov (Instituto de Geología, UNAM), and Gretchen Lapidus Lavine (Universidad Autónoma Metropolitana, Itzapalapa) for technical assistance. This research was supported in part by The National Autonomous University of Mexico [DGAPA-UNAM, PAPITT (Grant No. IN116007-2)], CONACYT [SEP-CONACYT Ciencia Básica 2006, Grant No. 61670], and the UC MEXUS Program. The original form of this manuscript was improved significantly thanks to comments by one anonymous reviewer, Dave Craw (U. Otago, New Zealand), D. Kirk Nordstrom (U.S. Geological Survey, Boulder, CO) and Rebecca Sutton (Environmental Working Group, Oakland, CA).

REFERENCES

Baes C. F. and Mesmer R. E. (1976) *The Hydrolysis of Cations*. Krieger Publishing Company, Malabar, FL, 489 pp.

Bottomley D. J. (1984) Origins of some arseniferous groundwater in Nova Scotia and New Brunswick. *Can. J. Hydrol.* **69**, 223–257.

Brown, Jr., G. E., Foster A. L. and Ostergren J. D. (1999) Mineral surfaces and bioavailability of heavy metals: a molecular-scale perspective. *Proc. Natl. Acad. Sci. USA* **96**(7), 3388–3395.

Craw D. and Pacheco L. (2002) Mobilization and bioavailability of arsenic around mesothermal gold deposits in a semiarid environment, Otago, New Zealand. *Sci. World J.* **2**, 308–319.

Cervini-Silva J. and Sposito G. (2002) Steady-state dissolution kinetics of aluminum–goethite in the presence of desferrioxamine-B and oxalate ligands. *Environ. Sci. Technol.* **36**, 337–342.

Cheah S. F., Kraemer S. M., Cervini-Silva J. and Sposito G. (2003) Steady-state dissolution kinetics of goethite in the presence of desferrioxamine B and oxalate ligands: implications for the microbial acquisition of iron. *Chem. Geol.* **198**, 63–75.

Chen C. J., Chuang Y. C., Lin T. M. and Wu H. Y. (1985) A retrospective study on malignant neoplasms of bladder, lung and liver in blackfoot disease endemic area in Taiwan. *Cancer Res.* **45**, 5895–5899.

Cocozza C., Tsao C. C. G., Cheah S. F., Kraemer S. M., Raymond K. N., Miano T. M. and Sposito G. (2002) Temperature dependence of goethite dissolution promoted by trihydroxamate siderophores. *Geochim. Cosmochim. Acta* **66**, 431–438.

Cornell R. M. and Schwertmann U. (2003) *The Iron Oxides. Structure, Properties, Reactions, Occurrences and Uses*. VCH Publishers, Weinheim.

Craw D., Falconer D. and Youngson J. H. (2003) Environmental arsenopyrite stability and dissolution: theory, experiment, and field observations. *Chem. Geol.* **199**, 71–82.

Cruz R., Lazaro I., Rodriguez J. M., Monroy M. and Gonzalez I. (1997) Surface characterization of arsenopyrite in acidic medium by triangular scan voltammetry on carbon paste electrodes. *Hydrometallurgy* **46**, 303–319.

De Giudici G., Rossi A., Fanfani L. and Lattanzi P. (2005) Mechanisms of galena dissolution in oxygen-saturated solutions: evaluation of pH effect on apparent activation energies and mineral–water interface. *Geochim. Cosmochim. Acta* **69**, 2321–2331.

De Giudici G., Ricci P., Lattanzi P. and Anedda A. (2007) Dissolution of the (0 0 1) surface of galena: an in situ assessment of surface speciation by fluid-cell micro-Raman spectroscopy. *Am. Mineral.* **92**, 518–524.

Elrick K. A. and Horowitz A. J. (1986) Analysis of rocks and sediments for arsenic, antimony, and selenium, by wet digestion and hydride generation atomic absorption. In *Varian Instruments at Work*. Number AA-56, 5 p.

Frost R. R. and Griffin R. A. (1977) Effect of pH on adsorption of arsenic and selenium from landfill leachate by clay minerals. *Soil Sci. Soc. Am. J.* **41**, 53–57.

Georgiadis M., Cai Y. and Solo-Gabriele H. M. (2006) Extraction of arsenate and arsenite species from soils and sediments. *Environ. Pollut.* **141**, 22–29.

Goldhaber M. B. (1983) Experimental study of metastable sulfur oxyanion formation during pyrite oxidation at pH 6–9 and 30 °C. *Am. J. Sci.* **283**, 193–217.

Greenwood N. N. and Earnshaw A. (1984) *Chemistry of the Elements*. Pergamon Press, Oxford.

Haack E., Johnston C. T. and Maurice P. A. (2006). In *Proceedings of the 232nd National Meeting of the American Chemical Society*, September 10–14. The American Chemical Society, San Francisco, CA.

Hernlem B. J., Vane L. M. and Sayles G. D. (1995) Stability constants for complexes of the siderophore desferrioxamine B with selected heavy metal cations. *Inorg. Chim. Acta* **244**, 179–184.

Hernlem B. J., Vane L. M. and Sayles G. D. (1999) The application of siderophores for metal recovery and waste remediation: examination of correlations for prediction of metal affinities. *Water Res.* **33**, 951–960.

Hersman L., Lloyd T. and Sposito G. (1995) Siderophore-promoted dissolution of hematite. *Geochim. Cosmochim. Acta* **59**, 3327–3330.

Holmén B. A. and Casey W. H. (1996) Hydroxamate ligands, surface chemistry, and the mechanism of ligand-promoted dissolution of goethite [α-FeOOH(s)]. *Geochim. Cosmochim. Acta* **60**, 4403–4416.

Holmén B. A., Sison J. D., Nelson D. C. and Casey W. H. (1999) Hydroxamate siderophores, cell growth and Fe(III) cycling in two anaerobic iron oxide media containing *Geobacter metallireducens*. *Geochim. Cosmochim. Acta* **63**, 227–239.

Kalinowski B. E., Liermann L. J., Givens S. and Brantley S. L. (2000) Rates of bacteria-promoted solubilization of Fe from minerals: a review of problems and approaches. *Chem. Geol.* **169**, 357–370.

Korte N. C. and Fernando Q. (1991) A review of arsenic(III) in groundwater. *Crit. Rev. Environ. Control* **21**, 1–39.

Kraemer S. M., Cheah S.-F., Zapf R., Xu J., Raymond K. N. and Sposito G. (1999) Effect of hydroxamate siderophores on Pb(II) adsorption and Fe release by goethite. *Geochim. Cosmochim. Acta* **63**, 3003–3008.

Kraemer S. M., Xu J., Raymond K. and Sposito G. (2002) Adsorption of Pb(II) and Eu(III) by oxide minerals in the presence of natural and synthetic hydroxamate siderophores. *Environ. Sci. Technol.* **36**, 1287–1291.

Kraemer S. M., Butler A., Borer P. and Cervini-Silva J. (2005) Biogenic ligands and the dissolution of iron bearing minerals in marine systems. *Rev. Mineral. Geochem.* **59**, 53–84.

Lengke M. F. and Tempel R. N. (2002) Reaction rates of natural orpiment oxidation at 25 to 40 °C and pH 6.8 to 8.2 and

comparison with amorphous As_2S_3 oxidation. *Geochim. Cosmochim. Acta* **66**(18), 3281–3291.

Liermann L. J., Kalinowski B. E., Brantley S. L. and Ferry J. G. (2000) Role of bacterial siderophores in dissolution of hornblende. *Geochim. Cosmochim. Acta* **64**, 587–602.

Martell A. E., Smith R. M. and Motekaitis R. J. (1995) *Critically Stability Constants Database*. NIST, vol. 2 Gaithersburg, MD.

Maurice P. A., Lee Y. J. and Hersman L. E. (2000) Dissolution of Al-substituted goethites by an aerobic *Pseudomonas mendocina* var. *Geochim. Cosmochim. Acta* **64**, 1363–1374.

Maurice P. A., Vierkorn M. A., Hersman L. E. and Fulghum J. E. (2001) Dissolution of well and poorly ordered kaolinites by an aerobic bacterium. *Chem. Geol.* **180**, 81–97.

McKibben M. A. and Barnes H. L. (1986) Oxidation of pyrite in low temperature acidic solutions: rate laws and surface textures. *Geochim. Cosmochim. Acta.* **50**, 1509–1520.

Merian E. (1991) *Metals and their Compounds in the Environment. Occurrence, Analysis and Biological Relevance*. VCH Publishers, Germany, pp. 87–93.

Moffett J. (1988) The determination of arsenic in non-silicate geological ore samples using a vapor generation accessory. In *Varian Instruments at Work*. Number AA-78, 4 p.

Monroy-Fernandez M. G., Mustin C., de Donato P., Barres O., Marion P. and Berthelin J. (1995) Occurrences at mineral–bacteria interface during oxidation of arsenopyrite by *Thiobacillus ferrooxidans*. *Biotechnol. Bioeng.* **46**, 13–21.

Moses C. O., Nordstrom D. K., Herman J. S. and Mills A. L. (1987) Aqueous pyrite oxidation by dissolved oxygen and by ferric iron. *Geochim. Cosmochim. Acta* **51**, 1561–1571.

Ng J. C., Wang J. and Shraim A. (2003) A global health problem caused by arsenic from natural sources. *Chemosphere* **52**, 1353–1359.

Nordstrom D. K. and Archer D. G. (2003). In *Arsenic in Ground Water: Geochemistry and Occurrence* (eds. A. H. Welch and K. G. Stollenwerk). Kluwer Academic Publishers, Boston, pp. 1–25.

O'Day P., Vlassopoulos D., Meng X. and Benning L. G. (eds.) (2005) *Advances in Arsenic Research: Integration of Experimental and Observational Studies and Implications for Mitigation*, 450 pp. ACS Symposium Series No. 915. American Chemical Society.

Palache C., Berman H. and Frondel C. (1944) *The system of mineralogy of James Dawght Dana and Edward Salisbury Dana*, seventh ed. .

Parkhurst D. L. (1995) User's guide to PHREEQC-A computer program for speciation, reaction-path, advective-transport, and inverse geochemical calculations. *USGS Water Resources Investigations Report*, 95-4227.

Pinto S. S. and Nelson K. W. (1976) Arsenic toxicology and industrial exposure. *Annu. Rev. Pharmacol. Toxicol.* **16**, 95–100.

Plant J. A., Kinniburgh D. G., Smedley P. L., Fordyce F. M. and Klinck B. A. (2005) Arsenic and selenium. In *Environmental Geochemistry: Treatise on Geochemistry* (ed. L. B. Sherwood). British Geological Survey, Nottingham, UK.

Rodríguez V. M., Jiménez-Capdeville M. E. and Giordano M. (2003) The effects of arsenic exposure on the nervous system. *Toxicol. Lett.* **145**, 1–18.

Rohwerder T., Gehrke T., Kinzler K. and Sand W. (2003) Bioleaching review part A: progress in bioleaching: fundamentals and mechanisms of bacterial metal sulfide oxidation. *Appl. Microbiol. Biotechnol.* **63**, 239–248.

Smith A. H., Lopiperom P. A., Bates M. N. and Steinmaus C. M. (2002) Arsenic epidemiology and drinking water standards. *Science* **296**, 2145–2146.

Solinas V. (1994) Cation effects on the adsorption of desferrioxamine B (DFOB) by humic acid. In *Humic Substances in the Global Environment and Implications on Human Health* (eds. N. Senesi and T. M. Miano). Elsevier, Amsterdam, pp. 1183–1188.

Steudel R. (1996) Mechanism for the formation of elemental sulfur from aqueous sulfide in chemical and microbiological desulfurization processes. *Ind. Eng. Chem. Res.* **35**, 1417–1423.

Stumm W. and Morgan J. J. (1996) *Aquatic Chemistry: Chemical Equilibria and Rates in Natural Waters*. Wiley, NY.

Telford J. R. and Raymond K. N. (1996) Siderophores. In *Comprehensive Supramolecular Chemistry*, vol. 1 (eds. J. E. Atwood, J. E. Davis, D. D. MacNicol and F. Vögtle). Elsevier, Oxford, p. 245.

Voigt D. E., Brantley S. L. and Hennet R. J. C. (1996) Chemical fixation of arsenic in contaminated soils. *Appl. Geochem.* **11**, 633–643.

Walker F. P., Schreiber M. E. and Rimstidt J. D. (2006) Kinetics of arsenopyrite oxidative dissolution by oxygen. *Geochim. Cosmochim. Acta* **70**, 1668–1676.

Watteau F. and Berthelin J. (1994) Microbial dissolution of iron and aluminum from soil minerals: efficiency and specificity of hydroxamate siderophores compared to aliphatic acids. *Eur. J. Soil Biol.* **30**, 1–9.

Zhang H., Penn R. L., Hamers R. J. and Banfield J. F. (1999) Enhanced adsorption of molecules on the surface of nanocrystalline particles. *J. Phys. Chem. B* **103**, 4656–4662.

Associate editor: James Kubicki